npj | spintronics

www.nature.com/npjspintronics

ARTICLE OPEN

Check for updates

Magnonic combinatorial memory

Mykhaylo Balinskyy[1] and Alexander Khitun[1]✉

In this work, we consider a type of magnetic memory where information is encoded into the mutual arrangement of magnets. The device is an active ring circuit comprising magnetic and electric parts connected in series. The electric part includes a broadband amplifier, phase shifters, and attenuators. The magnetic part is a mesh of magnonic waveguides with magnets placed on the waveguide junctions. There are amplitude and phase conditions for auto-oscillations to occur in the active ring circuit. The frequency(s) of the auto-oscillation and spin wave propagation path(s) in the magnetic part depends on the mutual arrangement of magnets in the mesh. The propagation path is detected with a set of power sensors. The correlation between circuit parameters and spin wave path is the basis of memory operation. The combination of input/output switches connecting electric and magnetic parts and electric phase shifters constitute the memory address. The output of the power sensors is the memory state. We present experimental data on the proof-of-the-concept experiments on the prototype with three magnets placed on top of a single-crystal yttrium iron garnet $Y_3Fe_2(FeO_4)_3$ (YIG) film. There are three selected places for the magnets to be placed. There is a variety of spin wave propagation paths for each configuration of magnets. The results demonstrate a robust operation with an On/Off ratio for path detection exceeding 35 dB at room temperature. The number of possible magnet arrangements scales factorially with the size of the magnetic part. The number of possible paths per one configuration scales factorial as well. It makes it possible to drastically increase the data storage density compared to conventional memory devices. Magnonic combinatorial memory with an array of 100×100 magnets can store all information generated by humankind. Physical limits and constraints are also discussed.

npj Spintronics (2024)2:2 ; https://doi.org/10.1038/s44306-023-00005-0

INTRODUCTION

Information and communication technologies generate vast amounts of data that will far eclipse today's data flows[1]. The global data will grow to 175 zettabytes (ZB) by 2025, according to the International Data Corporation[2]. Conventional storage systems may become unsustainable due to their limited data capacity, infrastructure cost, and power consumption[3]. For example, flash-memory manufacturers would need $\sim 10^9$ kg of silicon wafers even though the total projected wafer supply is $\sim 10^7$–10^8 kg[1]. There is an urgent need for increasing the data storage density (i.e., the number of bits stored per area). In the traditional process of improving the data storage density, better performance is achieved by the miniaturization of the data-storage elements. It stimulates a quest for nanometer-size memory elements such as DNA-based[4] or sequence-defined macromolecules[5]. At the same time, *memory architecture and the principles of data storage remain mainly unchanged for the last 50 years*.

As an example, we would like to refer to Random Access Memory (RAM). Figure 1A shows a high-level picture of RAM organization. The core of the structure is an array of memory cells where each cell stores one bit of information. There is a variety of memory cells exploiting different physical phenomena/devices/circuits for data storage, such as static RAM[6], dynamic RAM[7], magnetic RAM[8], etc. In all cases, RAM contains multiplexing and demultiplexing circuitry for cell addressing. Typically, the addressing of a required cell is accomplished by transistors electrically connecting the cell on the selected row/column with the output circuit. The correlation between the cell address and cell state is the essence of data storage in RAM. It is illustrated in Fig. 1B. It is shown in a table where the first column depicts the memory cell binary address. The second column in the table depicts the cell state (i.e., 0 or 1). Regardless of the physical mechanism of data storage (e.g., mechanical, electrical, magnetic), conventional memory devices make use of the individual states of memory cells. This is the common property of all existing RAMs. *The maximum number of bits stored in conventional memory is linearly proportional to the number of memory cells*. It is important to note that only one-row and one-column transistors are used for cell addressing. Other combinations (e.g., two rows and two columns, two rows and three columns, etc.) are not used as it does not provide any additional information. For instance, connecting multiple rows with a single column will result in logic state 1 if there is just one cell in the low resistance state. In other words, conventional memory does not use all possible addresses but only a fraction of it. This provides an intriguing possibility of increasing the data storage density by exploiting the collective states of memory cells along with a larger number of possible addresses.

Here, we consider the possibility of building a fundamentally different data-storage device, where information is stored in the *collective arrangement of memory cells*. It allows us to drastically increase the number of memory states compared to conventional memories. The rest of the work is organized as follows. In "Results", we describe the principle of operation of Magnonic Combinatorial Memory (MCM), present the results of numerical modeling illustrating MCM operation, and present experimental data obtained for the prototype. Then, we discuss the results and conclude on the potential advantages and shortcomings of MCM.

RESULTS

Principle of operation

To explain the essence of the combinatorial approach, we refer to the well-known combinatorial problem of counting paths in the grid. There are many possible ways to choose a path from one cell to another cell on a grid. It depends on the grid dimensions and the allowed steps of motion. Figure 2A shows a 2D mesh of cells

[1]Department of Electrical and Computer Engineering, University of California - Riverside, Riverside, California 92521, USA. ✉email: akhitun@engr.ucr.edu

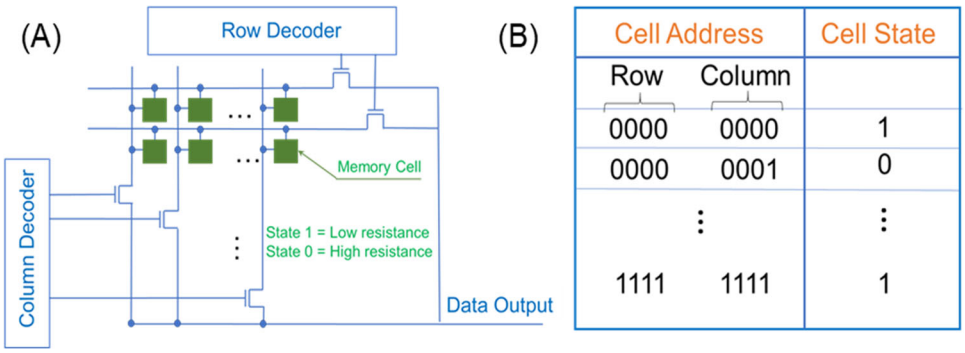

Fig. 1 Conventional RAM organization and truth table. A Schematics of RAM organization. There is a 2D mesh of memory cells arranged in rows and columns. The addressing of a required cell is accomplished by the row/column decoders. **B** Example of RAM truth table. The first column in the table depicts the memory cell binary address. The second column in the table depicts the cell state. The maximum number of bits stored is limited by the number of memory cells.

and a compass rose. The cells are connected to each other via vertical, horizontal, and diagonal lines. The compass rose displays the orientation of the cardinal directions on the grid, where steps in north, northeast, or east directions are allowed. The two numbers in each cell show the cell's coordinates. For instance, the cell in the southwest corner has coordinates (0,0), and the cell in the northwest corner has coordinates (3,3). In Fig. 2B, three possible paths from cell (0,0) to cell (3,3) are shown in red, green, and yellow color. These are just three possible paths out of many possible. The total number of paths from the southwest corner (0,0) of a rectangular grid to the northeast corner (m, n), using only single steps north, northeast, or east, is given by Delannoy numbers[9]:

$$D(m,n) = \sum_{k=0}^{\min(m,n)} \binom{m}{k}\binom{n}{k} 2^k, \tag{1}$$

where k is an integer, the binominal coefficients on the right side of the formula can be compactly expressed using factorial notation as follows:

$$\binom{m}{k} = \left(\frac{m!}{k!(m-k)!}\right), \binom{n}{k} = \left(\frac{n!}{k!(n-k)!}\right) \tag{2}$$

For instance, there are 63 paths connecting cells (0,0) and (4,4) in Fig. 2B. There are hundreds of unique paths as well as path combinations connecting cells on the left side to the cells on the right side of the grid. *The main idea of our approach is to exploit the huge number of paths in the grid for data storage*. Each path can be expressed as a binary number. For example, the path shown in red from (0,0) to (4,4) can be expressed as (1000 0100 0010 0001). *A binary number corresponding to the path can be considered as a memory state*. In contrast to 0 and 1 in conventional RAM, the output of combinatorial memory is a multi-digit binary number corresponding to one of the possible paths.

In order to make use of the multiple paths for data storage, one needs to introduce a correlation between the memory addresses and memory states (i.e., make a physical system where a signal propagation path depends on the input conditions). In Fig. 2C, there is shown a modified 2D 4×4 grid, where each cell introduces a frequency-dependent attenuation $L_{ij}(f)$ [dB] and a frequency-dependent phase shift $\Delta_{ij}(f)$ $[\pi]$ to the propagating signal (i.e., signal is a continuous sinusoidal wave). The subscripts denote the cell position in the grid. In this case, waves propagating through the different paths may accumulate different phase shifts and attenuation:

$$L_{path}(f) = \sum_{ij} L_{ij}(f), \Delta_{path}(f) = \sum_{ij} \Delta_{ij}(f), \tag{3}$$

where the summation is over all cells in the path. *The total phase shift/attenuation for each path depends on the mutual arrangement of memory elements in the mesh*. It is possible to have unique phase shifts/attenuation for different paths or to have some paths with the same phase shift/attenuation. The examples are described in ref. [10].

To retrieve information encoded in one or another path in the grid, we propose to utilize an active ring circuit whose schematics are shown in Fig. 3A. It consists of active and passive parts. The active part includes a voltage-tunable broadband amplifier and a voltage-tunable phase shifter. The passive part is a 2D grid, as shown in Fig. 2C. The parts are connected in series via the sets of switches on the left and right sides of the passive part. There are two conditions for auto-oscillations to occur in the circuit[11]:

$$G(V) + L(f) \geq 1, \tag{4.1}$$

$$\Psi(V) + \Delta(f) = 2\pi k, \textit{where } k = 1, 2, 3, \ldots \tag{4.2}$$

where $G(V)$ is the gain provided by the voltage-tunable amplifier, $L(f)$ is the signal attenuation in the grid, $\triangle(f)$ is the phase shift of the grid, and $\Psi(V)$ is the voltage-tunable phase shift of the electric part. The first Eq. (4.1) states the amplitude condition for auto-oscillations: the gain provided by the broadband amplifier should be sufficient to compensate for losses in the grid. The second equation states the phase condition for auto-oscillations: the total phase shift for a signal circulating through the ring circuit should be a multiple of 2π. In this case, signals come in phase every propagation round. It is important that the grid parameters are frequency-dependent. *The system starts with a superposition of all possible frequencies propagating through all possible paths. Only signals propagating on the resonant frequency(s)/resonant path(s) in the grid are amplified in the active ring circuit*. It takes just a few rounds of signal circulation in the ring circuit till the amplitude of the signal propagating through the resonant path goes to the maximum (i.e., saturation). Thus, signal propagation paths depend on the position of the phase shifter, as illustrated in Fig. 3B–D. A more detailed explanation of the selective signal amplification in a multi-path active ring circuit can be found in ref. [10].

Resonant propagation path(s) depends not only on the position of the phase shifter but also on the combination of left/right switches and the level of amplification $G(V)$. The number of resonant paths increases for higher amplification as condition (4.1) is satisfied for a larger number of frequencies. The correlation between the combination of switches and the external phase on one side and the propagation path on the other side is the base for combinatorial memory operation. Table 1 shows an example of the truth table of combinatorial memory. *The memory address is a multi-digit binary number that is related to the states of the switches and the position of the phase shifter*. The memory state is a multi-

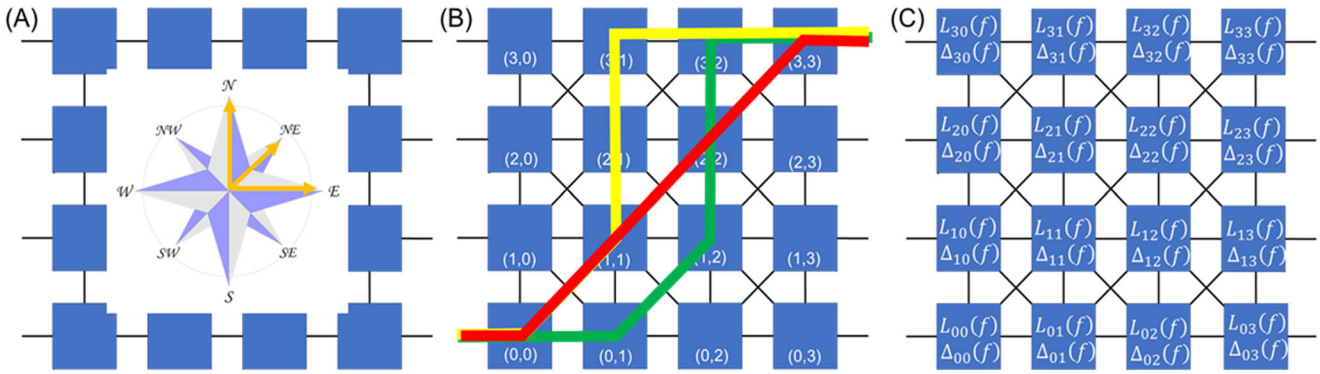

Fig. 2 Coding information in the paths on the grid. A A compass rose to display the orientation of the cardinal directions on the grid. Only steps in north, northeast, or east directions are allowed. **B** Schematics of a 4 × 4 grid. The red, green and yellow curves depict the three possible paths from the southwest corner (0,0) to the northeast corner (3,3). **C** Schematics of the modified grid where each cell introduces a frequency-dependent attenuation and a phase shift to the propagating wave.

digit binary number corresponding to the signal propagation path. In contrast to conventional RAMs using only a fraction of possible addresses, the proposed combinatorial memory exploits all the possible combinations of side switches (e.g., two switches in the On state on the left side and three switches in the On state on the right side). It does provide additional information as the grid impedance does depend on the connection configuration. The set of resonant paths with input ports #1 and #2 connected in parallel is not the sum of paths for port #1 and port #2 connected separately. The examples are presented in ref. [12]. The use of phase in addition to amplitude makes it possible to exploit a larger number of addresses compared to conventional memory.

In general, combinatorial memory can be implemented using different types of waves (e.g., acoustic, electric, optical). Here, we consider a *magnonic combinatorial memory* combining an active electric part and a passive multi-path magnonic part. There are several reasons for using spin waves. (1) Spin waves interact with magnets[13,14], which allows us to build a non-volatile memory (i.e., no energy is needed to keep magnets in a certain magnetization state). (2) Spin waves propagate much slower compared to electromagnetic waves, which allows us to achieve prominent phase shifts to the propagating signals[15]. (3) Magnet + magnonic waveguide acts as an efficient frequency filter for spin waves that allows us to exploit micromagnets as phase shifters and frequency filters at the same time[10].

The schematics of MCM are shown in Fig. 4. It is an active ring circuit where the passive part consists of a 5 × 5 mesh of magnonic waveguides shown in the light blue color. These waveguides are made of material with low spin wave dumping (e.g., yttrium iron garnet $Y_3Fe_2(FeO_4)_3$ (YIG)). There are magnets depicted by the blue-red rhombs placed on top of waveguide junctions. The magnets can be of different sizes and have several thermally stable states of magnetization. These magnets are aimed to act as the frequency filters and phase shifters for the propagating spin waves. Both the direction and the strength of the local magnetic field provided by the magnets are important for spin wave transport[16]. In the ideal scenario, all 25 magnets in the mesh provide different phase shifts and attenuation to the propagating spin waves. There are power sensors placed on top of the waveguides between the junctions. These sensors are aimed to detect the power of the spin wave signal and show the spin wave propagation paths. For example, it may be Inverse Spin Hall Effect (ISHE)-based sensors. Being of a relatively simple material structure (e.g., Pt wire on top of YIG waveguide), ISHE provides an output voltage proportional to the amplitude of the spin wave[17]. There are $(2n-1)\times n$ sensors in the mesh (i.e., there are 45 sensors shown in Fig. 4). Each sensor provides a voltage output V_{ij}, where subscripts i and j correspond to the row and column numbers, respectively. The magnonic mesh is connected to the electric part via the input and output ports located on the left and right sides of the mesh. The conversion from electromagnetic wave to spin wave and vice versa may be accomplished by micro antennas[18]. There is a switch (e.g., a transistor similar to one used in conventional memory for row/column addressing) at each input and output port to enable/disable the antenna for signal generation/receiving. These switches are aimed to control the combination of input/output antennas (e.g., input ports #2 and #3, output ports #1, #2, and #5). There are voltage-tunable frequency filters f_i, voltage-tunable phase shifters Ψ_i, and voltage-tunable attenuators A_i at each output port, where the subscript i depicts the output number. The voltage-tunable frequency filters are aimed to maximize the difference in the power on the different output ports. The phase shifters have discrete states corresponding to the specific phase shifts (e.g., $\Psi(0) = 0\pi$, $\Psi(1) = 0.25\pi$, $\Psi(2) = 0.5\pi$, etc.). The tunable attenuators are needed to tolerate possible structure imperfections and equalize the output spin wave power for all ports. There is one broadband amplifier G in the electric part.

Information in MCM is stored in the mutual arrangement of magnets in the mesh. There are $n!$ ways to have an ordered arrangement of n distinct objects[19]. Considering a set of n^2 distinct magnets in the mesh with n^2 junctions, the number of ordered arrangements (permutations) is given by

$$ordered\ magnet\ arrangements = (n^2)! \tag{5}$$

In turn, there are a number of spin wave propagation paths for *each of the magnet configurations*. The total number of paths can be calculated using Eq. (1). The number of paths in a real mesh may even exceed the Delannoy number as there is no restriction to spin waves to propagate in all possible directions (e.g., southwest, northeast, southeast). The number of paths just between the most distant cells scales as follows[12]:

$$number\ of\ paths\ (one\ input - one\ output) \approx (n+n)!/(n!\times n!). \tag{6}$$

The total number of paths from the left side (input) to the right side (output) of the mesh can be found by the summation of paths for all possible combinations of the input and output ports. There is an address assigned to each path. It includes a binary number corresponding to the states of the input switches, a binary number corresponding to the states of the output switches, and a binary number corresponding to the states of the phase shifters Ψ_i. The binary number for switches is an n-bit number, where 1 corresponds to the state On and 0 corresponds to the state Off. For example, the mesh shown in Fig. 4 has input ports #2, #3, and

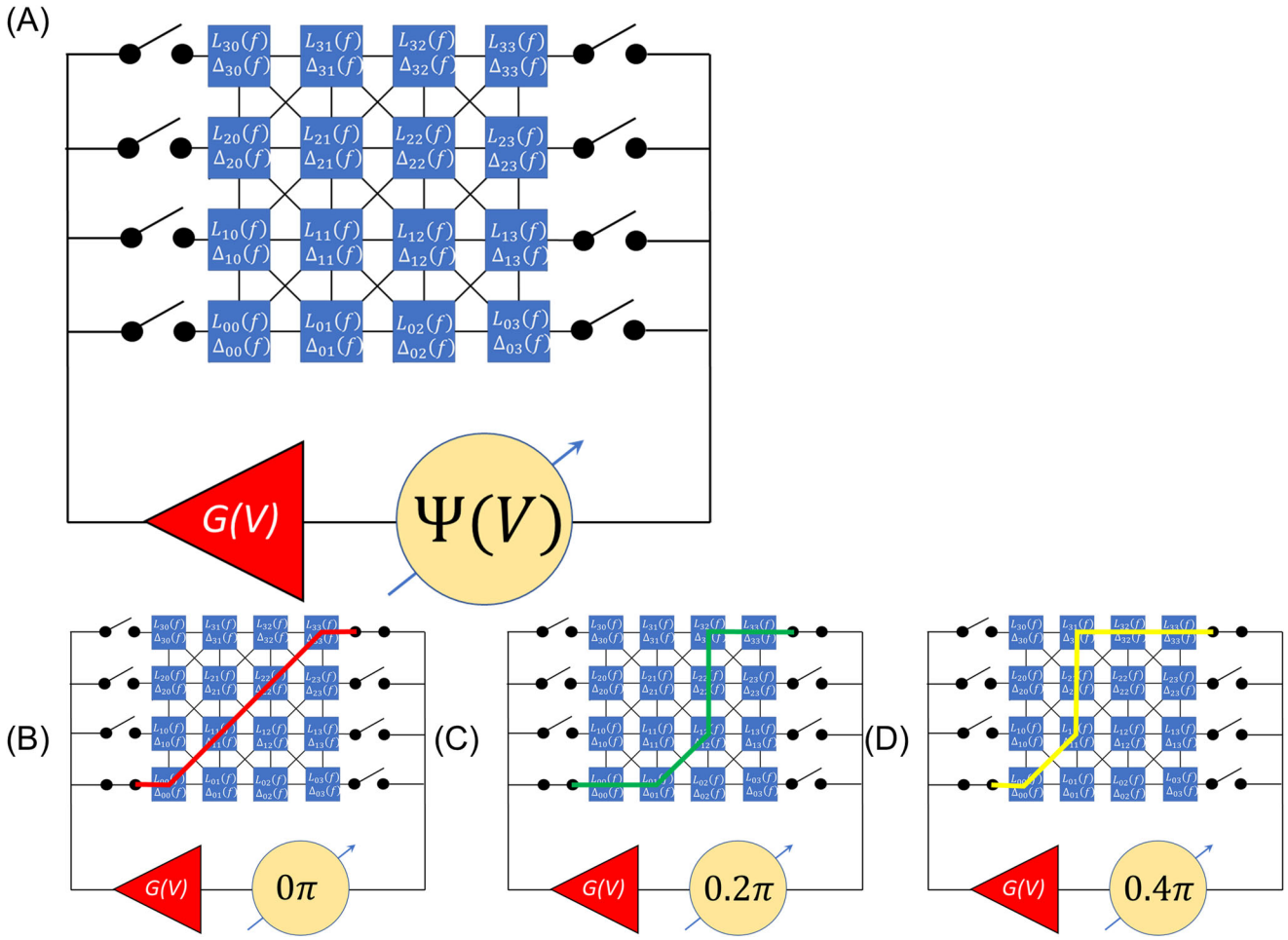

Fig. 3 Extracting paths using active ring circuit. A Schematics of a multi-path active ring circuit. The active part includes a voltage-tunable broadband amplifier $G(V)$ and a voltage-tunable phase shifter $\Psi(V)$. The passive part is the grid, as shown in Fig. 2C. Auto-oscillation occurs in the circuit when the active and passive paths are matched in amplitude and phase. **B**–**D** Illustration of the signal re-routing depending on the position of the voltage-tunable phase shifter. There are three paths shown for the three different positions of $\Psi(V)$: 0π, $0, 2\pi$, and 0.4π, respectively. The examples are shown only for one combination of the left/right switches.

Table 1. Example of the truth table of MCM.

Memory address	Memory state
001 001 0.0π	1001110010001101
001 001 0.2π	1100110000110001
001 001 0.4π	1010010000011000
.....	.....
001 001 1.8π	1011110001011000
011 011 0.0π	1011111100101101
011 011 0.2π	1100001001100101
.....	.....
011 011 1.8π	0000000000000000
011 011 0.0π	1101011100100101
011 011 0.2π	0101011000100111
.....	.....
111 111 1.8π	0101011010001110

The left column is the memory address, which includes the positions of the switches on the left and the right, the position of the phase shifter. The right column shows the memory state, which is the signal propagation path.

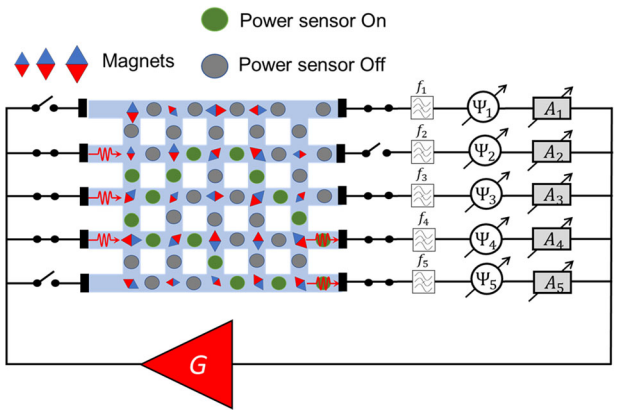

Fig. 4 Schematics of MCM. The core of the structure is a mesh of magnonic waveguides shown in the light blue color. There are magnets depicted by the blue-red rhombs placed on top of waveguide junctions. There are power sensors placed on top of the waveguides between the junctions. The mesh is included in an active ring circuit via switches on the left and right sides.

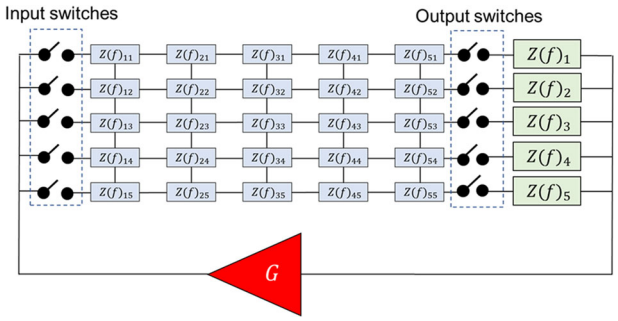

Fig. 5 Equivalent circuit for MCM. The mesh of waveguides with magnets is replaced with a mesh of cells with impedances $Z(f)_{ij}$, where subscripts i and j correspond to the column and row numbers, respectively. The real and the imaginary parts of each cell are frequency-dependent and correspond to the spin wave attenuation and phase shift accumulated while propagating through the junction. The output bandpass filters, phase shifters, and attenuators are replaced by the frequency depend on impedances $Z(f)_j$, where subscript j corresponds to the row number.

#4 in the position On. It corresponds to the binary address 01110. The output switches #1, #3, #4, and #5 are in the position On. It corresponds to the binary number 10111. The number of possible combinations of input switches is $2^n - 1$. It excludes one combination where all input ports are disconnected from the mesh. There is the same number of possible combinations of the output ports. There are more than two states for each phase shifter. In this case, the length of the binary number corresponding to the phase shifter states is related to z^n possible combinations, where z is the number of states per phase shifter. The total number of addresses is given as follows:

$$adresses = (2^n - 1)^2 \times z^n. \quad (7)$$

The memory state is the signal propagation path. It is recognized by the set of output voltages V_{ij} provided by the spin wave sensors. One may introduce a reference voltage V_{ref} to digitize the output. For instance, the output state is 1 if $V_{ij} \geq V_{ref}$, and 0 otherwise. Each path is described by $(2n-1) \times n$ bits. In the example shown in Fig. 4, the memory state is a sequence of 45 bits (one bit for each sensor). The total capacity of MCM is the product of the number of memory addresses and the number of bits stored per address that can be calculated as follows:

$$bits\ stored = (2^n - 1)^2 \times z^n \times n \times (2n - 1) \quad (8)$$

According to Eq. (7), the data storage capacity of MCM scales according to the power law with the size of the mesh. The data storage capacity of conventional memory scales linearly with the number of memory elements $n \times n$. It is important to note that the number of possible magnet arrangements given by Eq. (5) scales faster than the number of bits that can be addressed in Eq. (7). It may be possible to find an arrangement of magnets (i.e., one of many possible) that provides the desired spin wave propagation paths (i.e., information stored). The maximum number of unique phase addresses z^n in Eq. (7) is limited by the number of paths given by Eq. (6). It may be not practically feasible to utilize a number of phase states. Nevertheless, the number of information stored in MCM is skyrocketing even for a small number of phase states. For example, assuming $z = 4$ (i.e., four phases per phase shifter), MCM with 25 magnets $(n = 5)$ as shown in Fig. 4, can store up to 10 Mb of data. MCM with 100 magnets $(n = 10)$ can store up to 1 TB of data. MCM with a 100×100 $(n = 100)$ magnet array can store all the information generated by humankind.

Results of numerical modeling

The spin wave propagation path depends on the mutual arrangement of magnets in the magnonic mesh. This is the keystone of MCM operation. In order to illustrate it, we present the results of numerical modeling. Figure 5 shows an equivalent circuit for MCM. The mesh of waveguides with magnets is replaced with a 2D mesh of impedances. The real and the imaginary part of each cell corresponds to the spin wave attenuation and phase shift accumulated during propagation through the junction. Rigorously speaking, there should be additional cells in the mesh (i.e., impedances) to account for spin wave damping and accumulated phase shift during the propagation between the junctions. To simplify our consideration, we assume that the damping and the phase shift during the propagation between the junctions are much smaller compared to the ones during the propagation through the junction. The real and the imaginary parts of the junction impedances are frequency-dependent. Their values may be obtained from micromagnetic simulations[20] or from experiments[21].

There are three steps in the modeling procedure. First, one needs to find the total attenuation and the phase shift produced by the passive part *for all possible frequencies*. Second, the obtained results are checked to find the frequency(s) at which the self-oscillation conditions (4.1) and (4.2) are met. Finally, one needs to find the map of spin wave power flow through the mesh at the resonant frequency(s). The most time-consuming is the first step, as it takes a number of subsequent calculations to find the mesh responses in a wide frequency range. In order to speed up calculations and illuminate the essence of the proposed memory, we make several assumptions. (1) We assume that each propagation path in the mesh is associated with a certain propagation frequency. (2) The attenuation is linearly proportional to the propagation distance. (3) The junctions provide a frequency-independent phase shift. The objective is to show the change in the signal propagation paths depending on the arrangement of a given set of elements in the mesh.

In Fig. 6A, it is shown a mesh where numbers in the boxes show the phase shift accumulated by the propagating wave. It is assumed that the output attenuators are set to exclude the paths for more than six junctions (i.e., the amplitude condition is satisfied for all paths coming through five or six junctions). The output phase shifters are set to $\Psi = 0.5\pi$. The phase condition is satisfied for the paths providing 1.5π phase shift. The particular frequency(s) coming through these paths are of no importance. All the input and output switches are in the On state. The set of power detectors in Fig. 6A shows the signal propagation path for the given configuration of magnets. There are two paths. One path is from the input port #2 to the output port #1. The other path is from input port #5 to the output port #4. Let us change the places of two cells in the mesh. For example, we flip the two adjacent cells in the second row at columns two and three. It results in a change in the signal propagation path. In Fig. 6B, the green circles of power detectors show the paths. It is different from the one in Fig. 6A. The difference in the memory state is eight bits. It is possible to engineer magnonic meshes where the change in the position of just one magnet will lead to a multi-bit difference in the output. It should be noted that changing the mutual position of cells may or may not change the propagation routes in the mesh. An example is shown in the Supplementary materials.

Experimental data

In this part, we present experimental data obtained for the prototype with just three magnets. The schematics of the prototype are shown in Fig. 7A. It is a multi-path active ring circuit comprising electric and magnetic parts. The electric part consists of an amplifier (three amplifiers Mini-Circuits, model

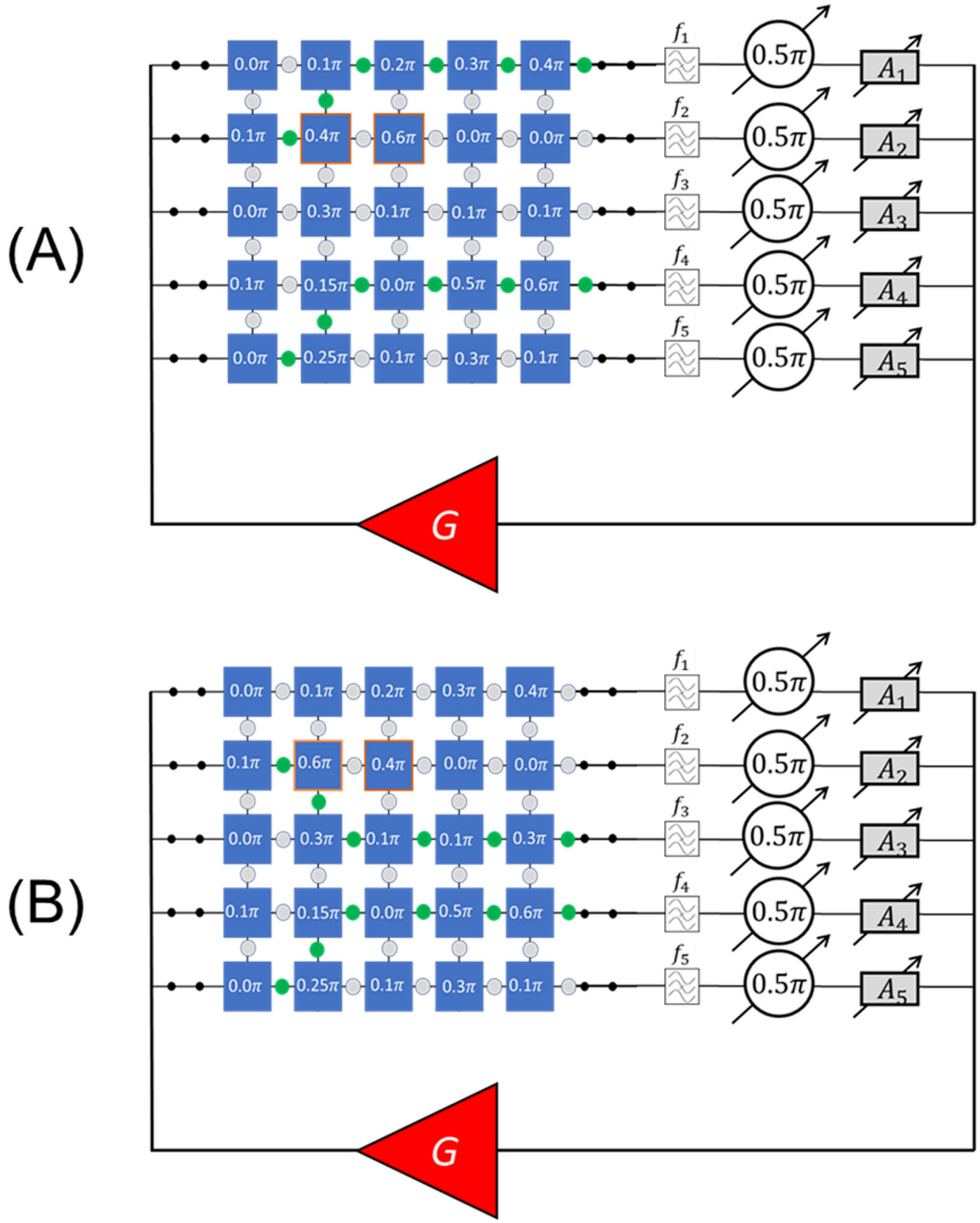

Fig. 6 Schematics of the simplified circuit model. The numbers in the boxes show the phase shift of the cell. The amplitude condition is satisfied for all routes coming through five or six junctions. The output phase shifters are set to $\Psi = 0.5\pi$. All input and output switches are in the On state. **A** The set of power sensors (green circles) shows the signal propagation paths for the given configuration of phase shifters. **B** The set of power sensors (green circles) shows the signal propagation paths where two cells are flipped in their positions (two adjacent cells in the second row at columns two and three).

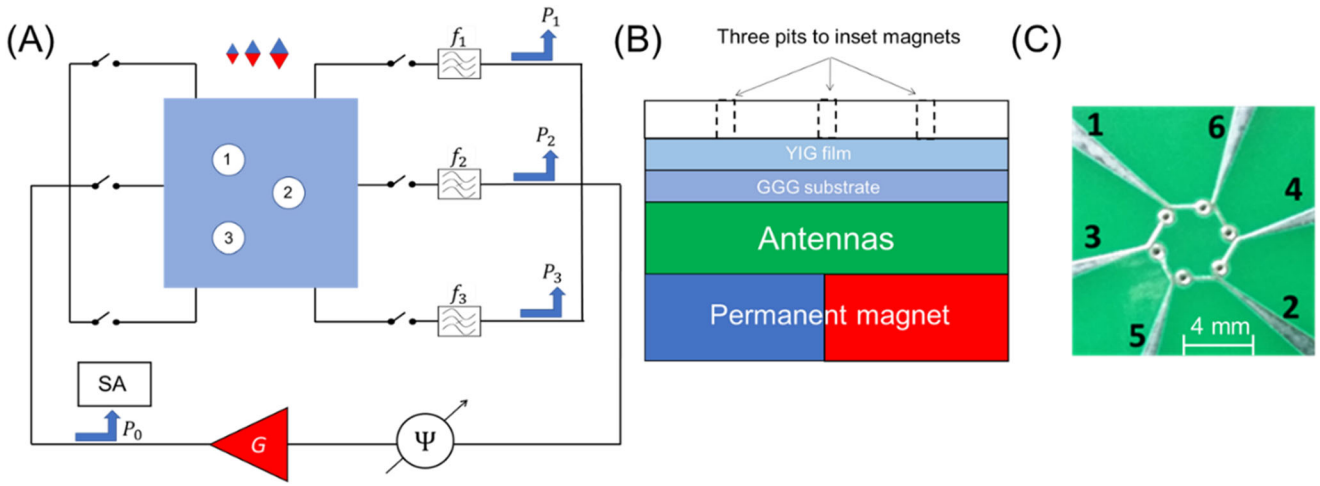

Fig. 7 First MCM with three magnets. A Schematics of the prototype. It is an active ring circuit comprising electric and magnetic parts. The magnonic part is a YIG film with three fixed places (i.e., depicted by the circles numbered 1, 2, and 3) for three different magnets to be placed on top of the film. There are three input and three output antennas to connect electric and magnetic parts. There are three voltage-tunable bandpass filters at the output ports. The filters at output ports #1, #2, and #3 are set to the central frequencies $f_1 = 2.539$ GHz, $f_2 = 2.475$ GHz, and $f_3 = 2.590$ GHz, respectively. **B** The cross-section of the passive magnonic part. It consists from the bottom to the top of a permanent magnet made of NdFeB, a Printed Circuit Board (PCB) substrate with six short-circuited antennas, a ferrite film made of GGG substrate and YIG layer, and a plastic plate with three pits for magnets to be inserted. The permanent magnet is aimed to create a constant bias magnetic field. **C** The photo of the PCB with six antennas. The characteristic size of the antenna is 2 mm in length and 0.15 mm in width.

ZX60-83LN-S+ connected in series) and a phase shifter (ARRA, model 9418A). The magnonic part is a ferrite film with three fixed places (i.e., depicted by the circles numbered 1, 2, and 3) for three different magnets to be placed on top of the film. There are three input and three output antennas to connect electric and magnetic parts. Each input/output port can be independently connected/disconnected. There are three voltage-tunable bandpass filters at the output ports. The filters are commercially available YIG-based frequency filters produced by Micro Lambda Wireless, Inc, model MLFD-40540. The experimental data on the filter transmission and phase delay can be found in the supplementary materials. The filters at output ports #1, #2, and #3 are set to the central frequencies $f_1 = 2.539$ GHz, $f_2 = 2.475$ GHz, and $f_3 = 2.590$ GHz, respectively. Magnonic and electric parts are connected via the set of splitters and combiners (i.e., SPLT 1-3, Sigatek SP11R2F 1527). The power at each output port and the total power circulating in the ring circuit is measured by the spectrum analyzer (SA) GW Instek GSP-827 connected to the circuit through a directional coupler (DC, KRYTAR, model 1850). There are four places of connection shown in Fig. 7A. P_0 is the total power in the circuit measured just after the amplifier, P_1, P_2, and P_3 are the powers measured at the output ports after signal propagation through the passive magnonic part. The signal is significantly damped after the passive part so the sum of P_1, P_2, and P_3 is not equal to P_0. SA is also used for detecting the frequencies of the auto-oscillations in the ring circuit. A more detailed schematics of the experimental setup with a detailed map of signal attenuation through the parts can be found in the Supplementary Materials.

The cross-section of the passive magnonic part is shown in Fig. 7B. It consists from the bottom to the top of a permanent magnet made of NdFeB, a Printed Circuit Board (PCB) substrate with six short-circuited antennas, a ferrite film made of GGG substrate and YIG layer, and a plastic plate with three pits for magnets to be inserted. The permanent magnet is aimed to create a constant bias magnetic field. Hereafter, we refer to this relatively big permanent magnet (model BX8×84 by K&J Magnets, Inc., dimensions $1.5'' \times 1.5'' \times 0.25''$) as a magnet in the text. The magnetic field produced by this magnet defines the frequency window as well as the type of spin waves that can propagate in the ferrite film. The bias field is about 375 Oe and is directed in-plane on the film surface. The photo of the PCB with six antennas is shown in Fig. 7C. The antennas are marked as 1,2,3,..6. The characteristic size of the antenna is 2 mm in length and 0.15 mm in width. The ferrite film is made of YIG grown by liquid epitaxy on a GGG substrate. YIG was chosen due to the low spin wave damping. The film is not patterned. The thickness of the film is 42 μm. The saturation magnetization is close to 1750 G, the dissipation parameter (i.e., the half-width of the ferromagnetic resonance) $\Delta H = 0.6$ Oe. The plastic plate is mechanically attached on top of the ferrite film. There are three pits drilled in the layer for placing the micromagnets. There are three NdFeB micromagnets of volumes 0.02 mm^3, 0.03 mm^3, and 0.06 mm^3, respectively. The magnets are placed inside plastic tubes of different colors. The smallest-volume magnet is placed into the tube of black color without a sticker. The tubes with the white and the red stickers correspond to the middle-volume and large-volume magnets, respectively. Hereafter, we refer to the micromagnets as Black (B), White (W), and Red (R). The photo of the devices with tubes can be found in the Supplementary Materials.

The first set of experiments was accomplished for the case with three input and three output antennas connected. Antennas marked # 3, #4, and #6 are used for spin wave excitation in the ferrite film. Antennas marked #1, #2, and #5 are used for detecting the inductive voltage produced by the spin waves at the output. The summary of experimental data is shown in Table 2. The first column shows the combination of input and output switches. For instance, (111) means that all three input antennas are connected to the electric part. The second column shows the position of the external phase shifter. The external phase is set to $\Psi = 0\pi$. The third column shows the magnet arrangement. For example, BWR means that B magnet (smallest) is inserted into pit #1, W magnet (medium) is inserted into pit #2, and R magnet (largest) is inserted into pit #3. Combination (000) stands for the case without magnets placed in the pits. The fourth column shows the frequencies of the auto-oscillations (i.e., measured by SA). It may be one or several frequencies at the same time. The fifth column shows the power of the auto-oscillation P_0 at different frequencies. For example, the numbers in the second row (+2 dBm and +4 dBm) correspond to the frequencies 2.590 GHz and 2538 GHz, respectively. The sixth column shows the power measured at the

Table 2. Raw experimental data obtained for different magnet configurations.

Switches input output	Phase [π]	Magnets arrangement	Auto-oscillation frequency [GHz]	$P_0(f)$ [dBm]	P_1, P_2, P_3 [dBm]	Memory State
111 111	0	000	2.590	+7.5	−27, −75, −73	100
111 111	0	BWR	2.590, 2.538	+2, +4	−30, −78, −27	101
111 111	0	BRW	2.475	+6	−78, −30, −71	010
111 111	0	WBR	2.539	−1	−72, −71, −39	001
111 111	0	WRB	2.539	+2	−75, −69, −37	001
111 111	0	RBW	2.590, 2.539	+3, +1	−39, −75, −37	101
111 111	0	RWB	2.539	−3	−81, −78, −36	001

The first column shows the combination of input and output switches. The second column shows the position of the external phase shifter. The third column shows the magnet arrangement. For example, BWR means that B magnet (smallest) is inserted into pit #1, the W magnet (medium) is inserted in pit #2, and the R magnet (largest) is inserted into pit #3. Combination (000) stands for the case without magnets placed in the pits. The fourth column shows the frequencies of the auto-oscillations (i.e., measured by SA). It may be one or several frequencies at the same time. The fifth column shows the power of the auto-oscillation P_0 at different frequencies. For example, the numbers in the second row (+2 dBm and +4 dBm) correspond to the frequencies 2.590 GHz and 2538 GHz, respectively. The sixth column shows the power measured at the three output ports, where three numbers in each row correspond to P_1, P_2, and P_3, respectively. The last column in the table shows the logic output. It is logic 1 if the output power exceeds −45 dBm and logic 0 otherwise.

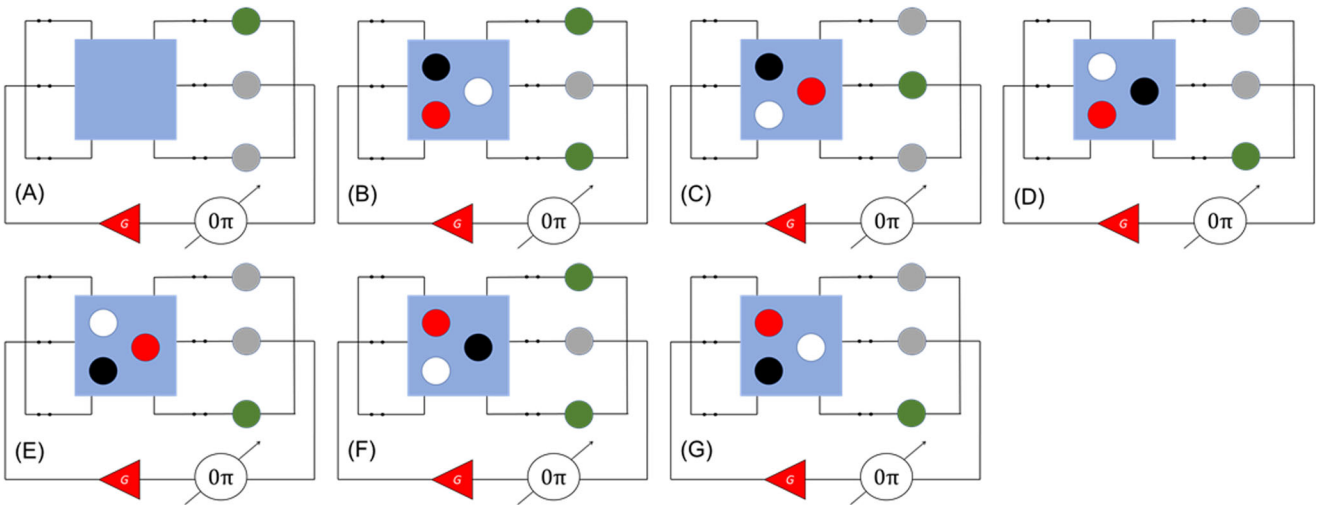

Fig. 8 Schematics of the circuit with magnet configuration and the output power distribution. The data taken for $\Psi = 0\ \pi$. The green circle depicts the output power exceeding −45 dBm, while the gray circle depicts the output power less than −45 dBm. **A** A film without magnets inserted. **B**–**G** All possible magnet combinations.

three output ports, where three numbers in each row correspond to P_1, P_2, and P_3, respectively. The output power ranges from −30 dBm to −79 dBm. The last column in the table shows the logic output. It is logic 1 if the output power exceeds −45 dBm and logic 0, otherwise. Power below the reference value is shown in blue color, while the power larger than the reference power is shown in red color. For example, −27 dBm, −75 dBm, −73 dBm in the first row correspond to the memory state 100. The data presented in Table 2 provides a detailed picture of the active ring dynamics, including the frequencies of auto-oscillation, the distribution of power between the frequencies, and the analog output at each port. There is no need to use SA in a practical device. All the collected data is aimed to explain the physical origin of data storage in MCM. The memory device will only provide binary output for the given binary address.

In order to visualize the data collected in Table 2, we show the schematics of the circuit with magnet configuration and the output power distribution in Fig. 8. The green circle depicts the output power exceeding −45 dBm, while the gray circle depicts the output power less than −45 dBm. The schematics in Fig. 8A correspond to the case without magnets inserted. Figure 8B–G shows all possible configurations of the magnets. One can see the difference in the output power for different magnet arrangements. The experiments were carried out for different positions of the phase shifter. The results obtained for $\Psi = 0.63\ \pi$. are shown in Fig. 9. The change of state of the external voltage-tunable phase shifter results in the spin wave re-routing in the ferrite film. The experiments were repeated for the different positions of the phase shifter. Raw data can be found in the Supplementary Materials. Experimental data on spin wave paths in the system with two input and three output antennas are also included in the Supplementary Materials.

DISCUSSION

There are two important observations we want to make based on the obtained experimental data. (1) Spin wave propagation path(s) depends on the configuration of magnets on top of the ferrite waveguide, the combination of input and output ports, and the output phase shifter. For instance, the arrangement of three different magnets or the arrangement of two different magnets with one empty pit results in different spin wave propagation paths. The reason for spin wave re-routing is the difference in the magnetic field profile on the top of the ferrite film that appears for the different arrangements of magnets. The re-routing can be modeled considering magnet/ferrite film as a bandpass filter and

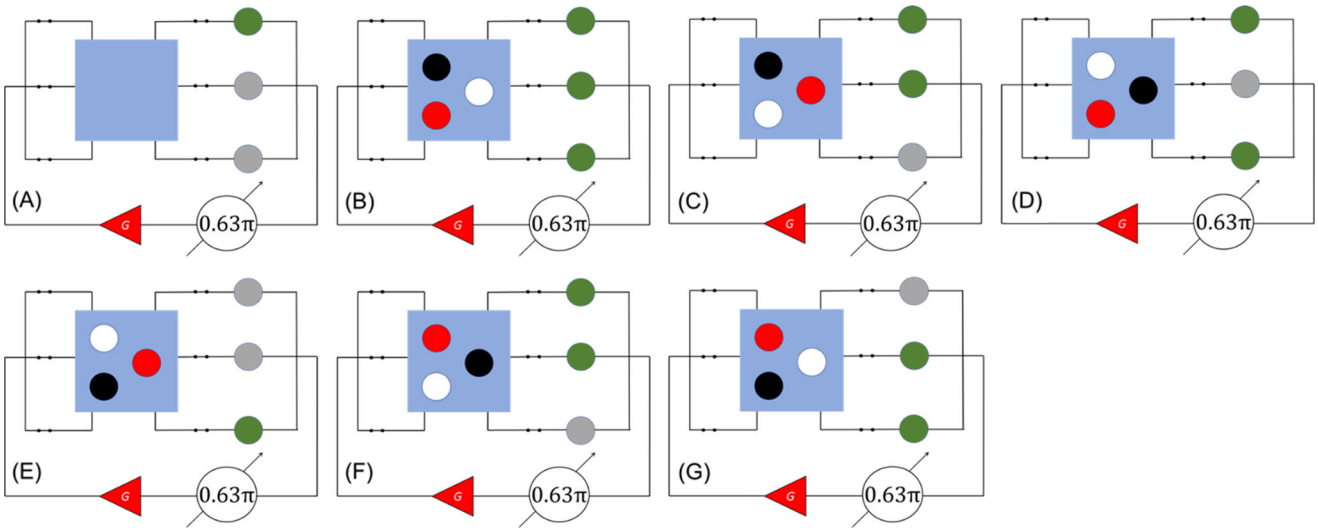

Fig. 9 Schematics of the circuit with magnet configuration and the output power distribution. The data taken for $\Psi = 0.63\ \pi$. The green circle depicts the output power exceeding −45 dBm, while the gray circle depicts the output power less than −45 dBm. **A** A film without magnets inserted. **B**–**G** All possible magnet combinations.

a phase shifter, as illustrated in the previous Section. However, high-fidelity numerical modeling would require an enormous deal of work to link the magnetic film properties to spin wave propagation paths in a wide frequency range. The external phase is an additional parameter that affects spin wave propagation in the active ring circuit. It makes a fundamental difference with conventional RAM, where low/high electric current is directly related to the high/low resistance states of the memory cells. In turn, the phase-dependent transport allows us to exploit the different combinations of input/output ports. Also, the addition of extra ports is not equivalent to the simple sum of paths and does not necessarily result in the additional paths. It may happen that some frequencies (paths) disappear for a larger number of inputs due to the spin wave interference.

(2) Spin wave propagation paths can be recognized by the set of power sensors with high accuracy. In the presented experiments, spin wave power was measured only at the output ports (i.e., no sensors within the mesh). The On/Off ratio (i.e., the difference between the outputs where most of the power flows and the outputs with minimum power) exceeds 35 dB at room temperature. It makes it possible to tolerate the inevitable structure imperfections, the difference in the efficiency of input/output antennas, etc. This big ratio is achieved by the introduction of frequency filters aimed to separate frequency responses between the different outputs. It may be possible to achieve an even bigger On/Off ratio by using filters with a smaller bandwidth. It will take an additional comparator-based circuit to digitize MCM output.

These observations confirm the main idea of this work on the feasibility of data storage using the mutual arrangement of magnets. It has the inherent advantages of traditional magnetic-based memory, including non-volatility and a long retention time. At the same time, MCM provides a fundamental advantage in data storage density compared to the existing memory devices. To comprehend this advantage, we summarized the data obtained for the same set of external phase shifters but with different configurations of magnets. Figure 10 shows the arrangement of magnets on the left and the corresponding truth tables for four phases on the right. There are three bits corresponding to the memory state in each row. Conventional memory with three magnets stores just three bits. It is the same amount of data that can be read out at one given phase in MCM (e.g., phase $= 0\ \pi$). All

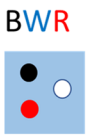

Input Phase [π]	Output State
0	101
0.63	111
1.25	010
1.75	001

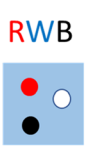

Input Phase [π]	Output State
0	001
0.63	011
1.25	110
1.75	011

Input Phase [π]	Output State
0	001
0.63	101
1.25	011
1.75	001

Fig. 10 Summary of experimental data obtained for different magnet combinations and four selected phases. On the left: the arrangement of magnets. On the right: the truth tables for four selected phases.

other rows (i.e., 3 out of 4 in each table) contain extra or exceed information compared to conventional RAMs. According to Eq. (8), the advantage over conventional data storage devices scales as the power law of the size of magnonic mesh $n \times n$.

There are several critical comments to mention. (1) The structure of the prototype is different from the general view MCM shown in Fig. 4. There are only three output ports in the prototype. The addition of power sensors within the magnetic part (e.g., between the magnets) would give a better picture of the spin wave path. It is also not clear if the ISHE sensors would need frequency filters for spin wave path detection. (2) The need to use different magnets (i.e., magnets providing different phase shift/amplitude changes to the propagating spin waves) significantly complicates the fabrication and initialization procedure. For instance, one has to have 25 different magnets to differentiate all possible paths in the device shown in Fig. 4. There are no

practical challenges associated with the fabrication of 25 magnets of different sizes or shapes on top of ferrite film. However, the change of the magnetization state after the fabrication becomes a very challenging problem. Theoretically, the post-fabrication initialization can be achieved using spin waves and specially engineered magnetic bits. In our preceding work, it was considered micro-structured magnetic bits for better interaction with spin waves[14]. We also want to refer to the recently reported nanomagnet reversal by propagating spin waves[22]. The switching was observed in ferromagnet/ferrimagnet hybrid structures consisting of $Ni_{81}Fe_{19}$ nanostripes prepared on top of YIG film. Alternatively, magnetization switching can be accomplished by all-optical tools without a magnetic field[23]. It may be a convenient way for MCM programming. Overall, the design and control of magnets in magnonic mesh is a complicated problem that requires special consideration.

It takes less than one millisecond for the prototype circuit to reach saturation. The estimated power consumption is about 1 μJ per 3-bit retrieval. The size of the magnetic part of the prototype is about 10×10 mm. There is a lot of room to reduce the retrieval time as well as the energy consumption. The time required for auto-oscillation to come to the steady-state regime depends on the parameters of the magnetic mesh and the characteristics of the amplifier[11]. The group velocity of magnetostatic spin waves is about 10^4 m/s. The read-out time can be minimized by the scaling down of magnonic mesh size. There are no physical constraints for scaling down the size of the magnets to the tens of nanometers[24]. It may be possible to place a 1000×1000 micro-magnet array on the 10×10 mm ferrite film. The scaling down can also minimize spin wave losses and reduce power consumption. MCM may not be capable of competing with conventional memory in the time of *single-bit* addressing or energy required for *single-bit* read-out. However, MCM enables a multi-bit read-out. The number of bits read out at a time by MCM scales proportional to the size of the mesh $n \times n$. It makes MCM efficient for a large mesh with a large number of cells.

The utilization of phase in addition to amplitude is the reason for data storage density enhancement in MCM. It opens a new dimension for information encoding. In this work, we considered an approach where multiple paths on the grid are differentiated by the accumulated phase shift. It is possible to have a unique phase shift for each of the possible paths (i.e., the phase shift of a cell is proportional to a prime number[10]). In turn, it increases the number of memory addresses one can use. Conventional memory devices (e.g., RAM) use only of a portion of possible cell addresses (i.e., one column/one row). MCM can utilize all possible combinations of input/output switches (e.g., the inputs /three outputs, four inputs, two outputs, etc.). The ability to control the phase shifters at each output port gives an additional degree of freedom. Overall, MCM provides a fundamental advantage in the data storage density compared to conventional memory devices.

From our point of view, the key question regarding MCM's potential implementation for data storage is associated with the feasibility of programming. *Is it possible to find a magnet arrangement for any given truth table?* It is an NP-hard problem to check all possible magnet configurations with the hope of finding the desired set of paths. The problem is further complicated by taking into consideration spin wave dispersion (spin wave spectra are shown in the Supplementary Materials) and the ability to choose a different set of phases and frequencies at each output. For instance, the experimental data obtained for the prototype were taken for the four phases (i.e., $\Psi(0) = 0\pi$, $\Psi(1) = 0.63\pi$, $\Psi(2) = 1.25\pi$, and $\Psi(3) = 1.75\pi$) and the set of three filter frequencies ($f_1 = 2.539$ GHz, $f_2 = 2.475$ GHz, and $f_3 = 2.590$ GHz). The change of the phase or the frequency may lead to a different set of paths. There is a plethora of possible combinations to be used for engineering the desired MCM output. The finding of the optimum set of parameters is another NP-hard problem to be solved.

There are certain disadvantages of the proposed MCM compared to conventional RAM. The bits in the conventional RAM are separate independently addressable discrete bits. It takes one operation to change one bit. In contrast, it may take the re-arrangement of all magnets in MCM just to change one bit in the stored massive array of data. That is the price to pay for using a collective state for information storage. Read-only memory is the most promising application for the proposed MCM, as the arrangement of magnets is fixed and is not modified after fabrication. There are many practical applications requiring high-density ROMs[25].

It may also be possible to utilize MCM as a RAM for some specific applications that deal with large sets of data (e.g., image processing[26]). It may take less time to re-arrange n magnets than to change one-by-one the states of $n!$ memory cells in conventional memory. It is important to develop a mechanism for fast and low-power consuming magnetization switching (e.g., all-optical magnetic switching[23]) to make MCM attractive for RAM applications. This and many other questions and concerns deserve special consideration. This work is aimed to introduce the concept of MCM and outline its potential advantages.

To conclude, we described a novel type of magnetic memory that is aimed to exploit the mutual arrangement of magnets for data storage. The principle of operation is based on the correlation between the arrangement of magnets on top of ferrite film and the spin wave propagation paths. The number of paths scales factorial with the number of magnets that makes it possible to encode more information compared to conventional magnetic memory devices exploiting the individual states of magnets. We presented experimental data on the proof-of-the-concept experiments on the prototype with just three magnets placed on top of a of single-crystal yttrium iron garnet $Y_3Fe_2(FeO_4)_3$ (YIG) film. The results demonstrate a robust operation with an On/Off ratio for path detection exceeding 35 dB at room temperature. This work is a first step toward the novel type of combinatorial memory devices that have not been explored. The material structure and principle of operation of MCM are much more complicated compared to conventional RAMs. At the same time, MCM may pave the road to unprecedented data storage capacity where a device with an array of 100×100 magnets can store all information generated by humankind.

METHODS

Device fabrication

The core of the device is made of single-crystal $Y_3Fe_2(FeO_4)_3$ film. The film was grown on top of a (111) Gadolinium Gallium Garnett ($Gd_3Ga_5O_{12}$) substrate using the liquid-phase epitaxy technique. The thickness of the film is 42 μm. The saturation magnetization is close to 1750 G, the dissipation parameter (i.e., the half-width of the ferromagnetic resonance) $\Delta H = 0.6$ Oe. The bias magnetic field is provided by the permanent magnet made of NdFeB.

Measurements

The excitation and detection of spin waves in the ferrite film was accomplished by six short-circuited antennas fabricated on PCB. The antennas are connected to a programmable network analyzer (PNA) Keysight N5241A. The filtering is by the commercially available filters produced by Micro Lambda Wireless, Inc., model MLFD-40540.

DATA AVAILABILITY

All data generated or analyzed during this study are included in this published article and the Supplementary Materials.

Received: 18 July 2023; Accepted: 23 November 2023;
Published online: 14 February 2024

REFERENCES

1. Zhirnov, V., Zadegan, R. M., Sandhu, G. S., Church, G. M. & Hughes, W. L. Nucleic acid memory. *Nat. Mater.* **15**, 366–370 (2016).
2. Reinsel, D., Gantz, J. & Rydning, J. *The Digitization of the World From Edge to Core* (Seagate, 2018).
3. Goda, K. & Kitsuregawa, M. The history of storage systems. *Proc. IEEE* **100**, 1433–1440 (2012).
4. Hao, Y. Y., Li, Q., Fan, C. H. & Wang, F. Data storage based on DNA. *Small Struct.* **2**, 2000046 (2021).
5. Martens, S. et al. Multifunctional sequence-defined macromolecules for chemical data storage. *Nat. Commun.* **9**, 4451 (2018).
6. Lin, Z. T. et al. A review on SRAM-based computing in-memory: circuits, functions, and applications. *J. Semicond.* **43**, 031401 (2022).
7. Nakagome, Y. & Itoh, K. Reviews and prospects of dram technology. *IEICE Trans. Commun. Electron. Inf. Syst.* **74**, 799–811 (1991).
8. Na, T., Kang, S. H. & Jung, S. O. STT-MRAM sensing: a review. *IEEE Trans. Circuits Syst. II-Express Briefs* **68**, 12–18 (2021).
9. Caughman, J. S., Haithcock, C. R. & Veerman, J. J. P. A note on lattice chains and Delannoy numbers. *Discrete Math.* **308**, 2623–2628 (2008).
10. Khitun, A. & Balinskiy, M. Combinatorial logic devices based on a multi-path active ring circuit. *Sci. Rep.* **12**, 9482 (2022).
11. Tiberkevich, V. S., Khymyn, R. S., Tang, H. X. & Slavin, A. N. Sensitivity to external signals and synchronization properties of a non-isochronous auto-oscillator with delayed feedback. *Sci. Rep.* **4**, 3873 (2014).
12. Balynsky, M. et al. Magnonic active ring co-processor. *J. Appl. Phys.* **133**, 023904 (2023).
13. Balinskiy, M. & Khitun, A. Micro magnet location using spin waves. *J. Appl. Phys.* **132**, 023902 (2022).
14. Balinskiy, M. & Khitun, A. Engineering structured magnetic bits for magnonic holographic memory. *AIP Adv.* **13**, 025245 (2023).
15. Balynsky, M. et al. A magnetometer based on a spin wave interferometer. *Sci. Rep.* **7**, 11539 (2017).
16. Gurevich, A. G. & Melkov, G. A. *Magnetization Oscillations and Waves* (CRC Press, 1996).
17. Balinskiy, M., Chiang, H., Gutierrez, D. & Khitun, A. Spin wave interference detection via inverse spin Hall effect. *Appl. Phys. Lett.* **118**, 242402 (2021).
18. Covington, M., Crawford, T. M. & Parker, G. J. Time-resolved measurement of propagating spin waves in ferromagnetic thin films. *Phys. Rev. Lett.* **89**, 237202 (2002).
19. Simovici, D. A. & Djeraba, C. *Mathematical Tools for Data Mining: Set Theory, Partial Orders, Combinatorics*. Advanced Information and Knowledge Processing, 529–549 (Springer, 2008).
20. Khitun, A. Parallel database search and prime factorization with magnonic holographic memory devices. *J. Appl. Phys.* **118**, 243905 (2015).
21. Balinskiy, M. et al. Spin wave interference in YIG cross junction. *AIP Adv.* **7**, 056633 (2017).
22. Baumgaertl, K. & Grundler, D. Reversal of nanomagnets by propagating magnons in ferrimagnetic yttrium iron garnet enabling nonvolatile magnon memory. *Nat. Commun.* **14**, 1490 (2023).
23. Stenning, K. D. et al. Low-power continuous-wave all-optical magnetic switching in ferromagnetic nanoarrays. *Cell Rep. Phys. Sci.* **4**, 101291 (2023).
24. Gertz, F., Kozhevnikov, A., Filimonov, Y. & Khitun, A. Magnonic holographic read-only memory. *IEEE Magn. Lett.* **7**, 3200204 (2016).
25. *Read-Only Memory (ROM) Market: Challenges, Opportunities, and Growth Drivers and Major Market Players Forecasted for Period from 2023 –2030* (ASPIRE RESEARCH, 2023); https://www.linkedin.com/pulse/read-only-memoryrom-market-challenges-opportunities-growth/.
26. Pietzsch, T., Saalfeld, S., Preibisch, S. & Tomancak, P. BigDataViewer: visualization and processing for large image data sets. *Nat. Methods* **12**, 481–483 (2015).

ACKNOWLEDGEMENTS

This work of M.B. and A.K. was supported in part by the INTEL CORPORATION, under Award #008635, Project director Dr. D. E. Nikonov, and by the National Science Foundation (NSF) under Award # 2006290, Program Officer Dr. S. Basu. The authors would like to thank Dr. D. E. Nikonov for the valuable discussions.

AUTHOR CONTRIBUTIONS

A.K. conceived the idea of magnonic combinatorial memory, designed the experiment, and provided numerical modeling. M.B. built the prototype and accomplished experiments. All authors reviewed the manuscript.

COMPETING INTERESTS

The authors declare no competing interests.

ADDITIONAL INFORMATION

Supplementary information The online version contains supplementary material available at https://doi.org/10.1038/s44306-023-00005-0.

Correspondence and requests for materials should be addressed to Alexander Khitun.

Reprints and permission information is available at http://www.nature.com/reprints

Publisher's note Springer Nature remains neutral with regard to jurisdictional claims in published maps and institutional affiliations.